Pulsed laval nozzle study of the kinetics of OH with unsaturated hydrocarbons at very low temperatures

Sally E. Taylor, Andrew Goddard, Mark A. Blitz, Patricia A. Cleary[a] and Dwayne E. Heard*

School of Chemistry, University of Leeds, Leeds, LS2 9JT, UK

Receipt/Acceptance Data **[DO NOT ALTER/DELETE THIS TEXT]**
Publication data **[DO NOT ALTER/DELETE THIS TEXT]**
DOI: 10.1039/b000000x [DO NOT ALTER/DELETE THIS TEXT]

The kinetics of reactions of the OH radical with ethene, ethyne (acetylene), propyne (methyl acetylene) and *t*-butyl-hydroperoxide were studied at temperatures of 69 and 86 K using laser flash-photolysis combined with laser-induced fluorescence spectroscopy. A new pulsed Laval nozzle apparatus is used to provide the low-temperature thermalised environment at a single density in N_2 of ~ 4×10^{16} molecule cm^{-3}. The density and temperature within the flow are determined using measurements of impact pressure and rotational populations from laser-induced fluorescence spectroscopy of NO and OH. For ethene, rate coefficients were determined to be k_2 = $(3.22 \pm 0.46) \times 10^{-11}$ and $(2.12 \pm 0.12) \times 10^{-11}$ cm^3 $molecule^{-1}$ s^{-1} at T = 69 and 86 K, respectively, in good agreement with a master-equation calculation utilising an *ab initio* surface recently calculated for this reaction by Cleary *et al*. (P. A. Cleary, M. T. Baeza Romero, M. A. Blitz, D. E. Heard, M. J. Pilling, P. W. Seakins and L. Wang, *Phys. Chem. Chem. Phys*., 2006, **8**, 5633-5642) For ethyne, no previous data exist below 210 K and a single measurement at 69 K yielded an upper limit for the rate coefficient of $k_3 < 1 \times 10^{-13}$ cm^3 $molecule^{-1}$ s^{-1}, consistent with the presence of a small activation barrier of ~ 5 kJ mol^{-1} between the reagents and the OH-C_2H_2 adduct. For propyne, there are no previous measurements below 253 K, and rate coefficients of k_4 = (5.08 ± 0.65), (5.02 ± 1.11) and $(3.11 \pm 0.09) \times 10^{-12}$ cm^3 $molecule^{-1}$ s^{-1} were obtained at T = 69, 86 and 299 K, indicating a much weaker temperature dependence than for ethene. The rate coefficient k_1 = $(7.8 \pm 2.5) \times 10^{-11}$ cm^3 $molecule^{-1}$ s^{-1} was obtained for the reaction of OH with *t*-butyl-hydroperoxide at T = 86 K. Studies of the reaction of OH with benzene and toluene yielded complex kinetic profiles of OH which did not allow the extraction of rate coefficients. Uncertainties are quoted at the 95% confidence limit and include systematic errors.

* *Corresponding author; email: d.e.heard@leeds.ac.uk*

a *Now at Department of Chemistry,University of Pennsylvania, Philadelphia, PA 19104, USA*

Introduction

The study of the kinetics of reactions at very low temperatures has important applications for understanding the chemistry of our own atmosphere and those of other planets, moons and comets, as well as processes occurring in dense interstellar clouds (ISCs) of star-forming regions. For exothermic radical-molecule reactions occuring on potential surfaces with very small or no activation barriers, non-Arrhenius behaviour is often observed.[1] The measurement of rate coefficients at very low temperatures and comparison with theoretical calculations is a very sensitive probe of our understanding of the chemical mechanism and the details of the intermolecular potential energy surface, particularly at long-range, where weakly bound van der Waals complexes have been observed.[2]

One important class of reactions in ISCs (T = 10 - 50 K) and the atmospheres of the outer planets or their satellites (e.g. Titan, 70K at its tropopause) is between free-radicals and unsaturated hydrocarbons. Smith et al.[2] have suggested that reactions of this type are likely to be fast at very low temperatures if the difference between the ionisation energy (IE) of the unsaturated molecule minus the electron affinity (EA) of the free-radical is less than ~ 9 eV. This rule is based on semi-empirical arguments and correlations of room temperature rate coefficients, and stems from the barrier height being dependent upon an avoided crossing between the neutral ground-state and an ionic excited state. Initially at large intermolecular distances the OH and unsaturated molecule will form a weakly bound van der Waals complex, and only if rearrangement of this to form a chemically bound adduct occurs via a submerged barrier (barrier is below the reagent asymptote) will the reaction be fast at very low temperatures.[2, 3]

In this paper we report rate coefficients at low temperature for reactions of OH with ethene, ethyne and propyne, all of which have been observed in ISC[4] and planetary atmospheres[5]. The reactions proceed via addition of OH to the double or triple bond forming a stable adduct, which is either stabilised by collisions or dissociates back to the reagents, leading to a pressure dependent rate coefficient. Decomposition of the adduct to other products is also possible, but only via an activation barrier, and this route is not favoured at low temperatures. Titan has a reducing atmosphere and hydrocarbons, measured from earth-based telescopes or more recently during the descent of the Huygens probe during the Cassini mission, are significant.[6] The influx of micrometeoroids in Titan's atmosphere provides a source of oxygen, with the incoming material, which is likely to be icy in nature, subliming in the thermosphere to deliver water vapour, which after photolysis or electron impact provides a source of OH radicals[5, 7] Ethyne is an important constituent of Saturn's atmosphere[8] (T=85 K at the tropopause). OH has an electron affinty of 1.827 eV [2] and so for ethene, propyne and ethyne the value of IE-EA is 8.7, 8.5 and 9.6 eV, respectively. The Smith et al. rule [2] therefore suggests that the former two, but not the latter, should be fast at very low temperatures.

Maintaining a thermalised environment at very low temperatures for kinetic studies has been achieved using either cryogenic cooling[9] or a supersonic gas expansion, and the methods have been extensively reviewed[4, 10, 11]. Cryogenic cooling of the reaction cell and using collisions with a buffer gas to cool the reagents has been widely used but suffers from the major drawback that many reagent gases, or particularly the precursors used to generate free-radicals, condense or adsorb onto walls of the chamber. Very low partial pressures of these gases must be used well below their saturated vapour pressures.

Free-jet supersonic expansions through a small orifice have enjoyed considerable success for spectroscopic studies, but only limited success for the study of kinetics at very low temperatures (0.1 – 20 K, mainly ion-molecule, for a review see [12]) due to the very steep spatial gradients in temperature and density as the gases move away from the nozzle. It is difficult to validate whether thermal equilbrium has been achieved in all parts of the flow, a necessary pre-requisite for kinetic studies, and considerable numerical modelling is required to extract rate coefficients. Rowe demonstrated that expansion through a Laval nozzle produced a flow of gas extending a considerable distance in which the temperature and density were uniform, and importantly, at thermal equilibrium[13]. The gas flow did not encounter the walls of the chamber, avoiding condensation problems, and the residence time in the flow was long enough to monitor a chemical reaction. The technique, known as CRESU (Cinétique de Réaction en Ecoulement Supersonique Uniforme), was initally used to measure rate coefficients for ion-molecule reactions[14], but its application was extended to the study of neutral-neutral reactions by Rowe, Sims and Smith, who generated free-radicals using laser flash photolysis (LFP) and monitored their temporal decay using laser-induced fluorscence (LIF) spectroscopy[1, 15, 16] or by chemiluminescence.[17,18] The method has enjoyed considerable success, and has been extensively reviewed.[2, 4, 10, 11] By heating the reservoir region prior to the Laval nozzle, the method has recently been used to study reactions of non-volatile species, for example polyaromatic hydrocarbons.[19, 20]

The CRESU technique uses a continuous flow of gas and although able to produce temperatures down to 7 K [1] requires very large pumps and enormous flows of gases. A continuous system with a modest pumping capacity using short Laval nozzles has recently been developed and able to generate temperaures as low as 77 K.[21] In order to reduce pumping capacity and gas flow considerably further, a number of pulsed CRESU systems have been developed, in which a short pulse of gas is expanded through the Laval nozzle,[22-26] achieving temperatures as low as 58 K,[25] and the reaction initiated and monitored using LFP-LIF.

In this paper we describe the pulsed Laval nozzle apparatus developed in Leeds and the results of experiments to characterise the spatial and temporal variation of temperature and density within the supersonic flow. The measurement of rate coefficients are presented for the following reactions:

$$OH + (CH_3)_3COOH \xrightarrow{k1} \text{products} \quad (1)$$

$$OH + C_2H_4 \xrightarrow{k2} \text{products} \quad (2)$$

$$OH + C_2H_2 \xrightarrow{k3} \text{products} \quad (3)$$

$$OH + C_3H_4 \xrightarrow{k4} \text{products} \quad (4)$$

$(CH_3)_3COOH$ is *t*-butyl-hydroperoxide (referred to here as *t*-BuOOH) and is the precursor used to generate OH. The experimentally determined values are compared, where possible, with previous measurements, and for C_2H_4 are also compared with master equation calculations using recently determined potential energy surfaces.[3, 27] Experiments are also described in which an attempt was made to measure rate coefficients for OH+benzene and OH+toluene at low temperatures in the Laval expansion.

Experimental

As this is the first paper describing the Leeds pulsed Laval supersonic nozzle apparatus with laser-induced fluorescence detection for kinetic studies, it is described in some detail. The overall design is based on the pulsed version of a CRESU apparatus pioneered by M. Smith and co-workers[24, 28], and subsequently adopted by the groups of Leone[22, 23] and Abel.[25] The design is influenced by experience gained by the authors during the operation of continuous [6] and pulsed[23] Laval nozzle systems. A schematic of the overall experimental arrangement of the apparatus is shown in Figure 1, consisting of a vacuum chamber and pumps, gas delivery system and reservoir, Laval nozzle, photolysis and probe laser systems, fluorescence collection system and data acquistion system. Each of these components are described in turn below.

Vacuum chamber and pumping arrangement

The main chamber is a 774 mm long stainless steel cylinder, of 3 mm thickness, capped at either end by a 240 mm diameter stainless steel flange (Leybold DN ISO-K250), as shown in Figure 1(a). The cylinder was manufactured by rolling a sheet of 3mm thick 316 stainless steel (fabricated by TEC Manufacturing Ltd.). Cut into the cylinder are six 160 mm diameter access ports each with individually adapted 160 mm diameter stainless steel flanges (Leybold DN ISO-K160). The 160 mm flanges, labelled 1-6 in Figure 1(a), are positioned to produce a 4-way and 6-way cross on the main cylinder, and each serve a particular purpose, as detailed in the caption to Figure 1(a). A 40 mm diameter access port adjacent to flange 4 allows electrical connections to a small stepper motor (Standa 004784, with in house motor controller) that translates a differential pressure transducer (Omega PX170-07DV) perpendicular to the gas flow in order to measure transverse profiles of impact pressure. The port is also used to feed through ¼ inch tubing connecting the pressure transducer to its vacuum reference. The pressure in the chamber is monitored by two capacitance manometers (Leybold CTR 90, 0-1000 and 0-10 Torr) and an ion gauge (Leybold Ionivac ITR 090).

The pumping system consists of a rotary pump (Leybold D65B) backing a Roots blower (Leybold RUVAC 251), connected to one of the large flanges of the main chamber by 63 mm diameter stainless steel tubing and bellows to minimise transfer of vibration. The pumps generate a pumping capacity of 210 $m^3\ hr^{-1}$ whilst maintaining a base pressure of 10^{-5} mBar. An adapted gate valve (Leybold DN63150-F H) is used to throttle the pumps and vary the pressure within the main chamber. For experiments using a Mach 4 nozzle, a second Roots blower (Edwards EH250) operated in parallel to the first, and backed by its own rotary pump (Edwards ED660), was used to increase pumping capacity.

Gas delivery system and reservoir

The carrier, radical-precursor and reagent gases all flow into the main chamber via the Laval nozzle which is immediately downstream of a small reservoir. The flow and hence partial pressure of each gas is controlled separately by mass flow controllers (MFC) (MKS Instruments) which are calibrated regularly. The total flow-rate of gas is 1000-2000 sccm, and after passing through the MFC, the gases pass through 2 m of ¼ external diameter stainless steel tubing before being mixed in a 2 litre stainless steel cylindrical ballast tank. The pressure in the ballast tank is monitored (MKS Baratron 0-5000 Torr) and provides a stable backing pressure for two solenoid valves (Parker series 9, normally closed, 24Vdc, stainless steel body, 0.116 inch orifice), which are each linked to the tank by a short section of ¼ inch external diameter stainless steel tubing passing through flange 2 (Figure 1(a)), and within the chamber by a short section of Teflon tubing to provide some flexibility. The pulse repetition frequency and duration of the opening of the valves is controlled using a pulse/delay generator (Berkeley Nucleonics Corporation 555) under computer control, and the required driver voltage and current supplied using a home-built power supply.

When open, a flow of gas from each valve is introduced into a small stainless steel pre-expansion reservoir, which is a 10 mm long, 10 mm diameter cylinder of volume of 0.78 cm^3, with apertures on the side for the pressure transducer and valves, but these are negligible in volume. The reservoir allows the pressure to build up prior to expansion through the Laval nozzle, which is connected to the front of the reservoir. A small internal volume piezo-resistive pressure transducer (Omega PX170-DE, 28 inch H_2O) is mounted to the top of the reservoir to monitor the temporal details of each gas pulse. The back of the reservoir is sealed with a 25 mm diameter quartz window to enable laser radiation to pass axially along the chamber. The reservoir has the capability to be cooled or heated by passing a silane-based thermofluid (Jencons) through its jacketed walls, with temperature control achieved using a circulating thermostat (Huber Unistat 360). However, the reservoir was not heated or cooled in this work, rather always held at room temperature.

The reservoir/nozzle assembly are mounted on a moveable yoke, which allows the axial distance from the exit plane of the Laval nozzle to the fluorescence detection region to be varied from 0 – 30 cm. Movement of the reservoir/nozzle is achieved using a stepper motor (McLennan) under computer control, which turns a threaded rod, upon which a second yoke is mounted outside the main chamber. Three rods attached to this yoke pass through gas-tight seals on the large end flange of the chamber and are bolted to the yoke upon which the reservoir is mounted within the chamber. As the threaded rod is turned one way or the other the yoke and hence the reservoir are translated either towards or away from the fluorescence region with an accuracy of ~ ± 1 mm.

Materials used: Nitrogen (BOC oxygen free), *t*-butyl-hydroperoxide (Sigma Aldrich, 70% v/v aqueous), nitric oxide (Air Products, 99.5%), ethene (Sigma Aldrich, > 99.5%), ethyne (BOC > 99.5%), propyne (Sigma Aldrich > 99.5%), benzene (Sigma Aldrich, >99.9%, HPLC grade) and toluene (Riedel-de Haën, >99.7%).

The Laval nozzle

From the reservoir the gas passes through the convergent section of the Laval nozzle, culminating in a narrow throat, before entering the divergent section where expansion of the gas, acceleration to supersonic velocities and cooling occurs. For a given throat diameter, length and curvature of the convergent and divergent sections, and a given carrier gas, a supersonic flow of approximately constant temperature and density is generated, extending tens of cm downstream of the nozzle, and providing a suitable environment for the study of low-temperature kinetics. The expansion is cylindrically symmetric and the shape of the divergent section is designed to remove unwanted secondary expansion waves. For an isoentropic flow, the final Mach number, *M* (flow velocity divided by local speed of sound), is given by the Rayleigh equation:

$$\frac{P_i}{P} = \left[\frac{(\gamma+1)M^2}{2}\right]^{\frac{\gamma}{\gamma-1}} \left(\frac{\gamma+1}{2\gamma M^2-\gamma+1}\right)^{\frac{1}{\gamma-1}} \qquad \text{(E1)}$$

where P_i and P are the impact pressure and static flow pressure, respectively, at a given point in the flow, and $\gamma = C_p/C_v$ is the ratio of specific heat capacities, which for the carrier N_2 gas used in this work is 7/5. In practice, the stagnation pressure P_o in the pre-expansion region of the reservoir and the impact pressure P_i are measured, which are related to M by:

$$\frac{P_i}{P_o} = \left[\frac{(\gamma+1)M^2}{(\gamma-1)M^2+2}\right]^{\frac{\gamma}{\gamma-1}} \left(\frac{\gamma+1}{2\gamma M^2-\gamma+1}\right)^{\frac{1}{\gamma-1}} \qquad \text{(E2)}$$

A trial value of M is chosen and its value optimised iteratively in order to find the value which best matches the measured value of P_i/P_o. All other properties of the flow can be calculated from M, using:

$$\frac{T}{T_o} = \left[1+\left(\frac{\gamma-1}{2}\right)M^2\right]^{-1} \qquad \text{(E3)}$$

$$\frac{P}{P_o} = \left[1+\left(\frac{\gamma-1}{2}\right)M^2\right]^{\frac{-\gamma}{\gamma-1}} \qquad \text{(E4)}$$

$$\frac{\rho}{\rho_o} = \left[1+\left(\frac{\gamma-1}{2}\right)M^2\right]^{\frac{-1}{\gamma-1}} \qquad \text{(E5)}$$

where T_o, P_o and ρ_o are temperature, pressure and density in the stagnation region of the reservoir and T, P and ρ are the corresponding values in the supersonic flow. Ideally the static flow pressure P should be the same as the background pressure in the chamber.

A computer program, developed by the group of M. Smith[24] was used to calculate the shape, throat diameter and dimensions of the Laval nozzles. The design of each nozzle is optimised to generate a specific final Mach number and hence temperature and density for N_2, given a set of input parameters. Details of the underlying equations which determine the precise nature of each nozzle, and the development of the flow characteristics during the expansion can be found elsewhere.[24]. The nozzles, which are removable and can be exchanged, have M values between 2.25 and 4, with design temperatures and densities between 71-148 K and 5-50×10^{16} molecule cm^{-3}. The actual performance characteristics of the two nozzles used in this work are given in the results section below.

Laser-flash photolysis and probe laser systems

OH radicals are generated via 248 nm KrF excimer laser (Lambda Physik LPX 200) photolysis of *t*-butyl-hydroperoxide. The laser beam was directed into the main chamber using dielectrically coated mirrors and an 8 mm diameter iris, where it counterpropagates axially with the gas flow and passes through the throat of the Laval nozzle and reservoir and through another window, held at Brewster's angle, before exiting the chamber, as shown in Figure 1. The excimer laser was equipped with unstable resonators in order to improve the collimation of the 248 nm laser beam. This laser beam was directed along the gas flow with a diameter of 8 mm at the crossing-point with the probe laser, and has a pulse energy of ~ 25 mJ $pulse^{-1}$ inside the chamber. The 248 nm beam diameter is just smaller than the diameter of the nozzle throat to minmise the reflection of scattered light back into the chamber. Outside the chamber the 248 nm laser beam is directed, after attenuation, onto a fast silicon photodiode, in order that the OH laser-induced fluorescence signal can be normalised for fluctuations in photolysis laser pulse energy. It was found, however, that the pulse-to-pulse stability of the 248 nm radiation is very good (< 5 %), and for most experiments was not monitored in this way, rather being directed to a beam dump. Instead, a power meter mounted within the excimer laser continously monitored the laser power, whose output was regularly checked.

The probe laser radiation entered the chamber in one of two ways, depending on the experiment being conducted. During some of the experiments to characterise the rotational temperature within the expansion, when nitric oxide in trace amounts in the carrier gas was used as the thermometer with laser-excitation of NO at 226 nm via the $A^2\Sigma^+$-$X^2\Pi$ (0,0) γ-band transition, no photolysis laser was necessary, and the probe laser entered the chamber in the manner described above. The 226 nm radiation was generated by a Nd:YAG laser (Spectron Lasers SL803) whose 355 nm output pumped a dye laser (Sirah Gmbh, Cobra Stretch) operating with Coumarin 47 dye to generate 452 nm, which after frequency doubling in a BBO crystal generated 226 nm radiation (~0.5 cm^{-1} linewidth), which was directed to the chamber via two prisms, and finally by reflection from a quartz plate to ensure the pulse energy in the chamber (< 0.5 mJ $pulse^{-1}$), is sufficiently small to prevent optical saturation of the NO laser-excitation spectrum. No lens was used to collimate the 226 nm radiation, and at the fluorescence collection region the beam was ~ 2 mm in diameter. A photodiode outside of the chamber, masked by a bandpass filter (UG-5) in order to block any residual 452 nm radiation, was used to monitor the relative 226 nm pulse energy for subsequent normalisation on a shot-to-shot basis.

For experiments involving generation of OH via flash-photolysis, the probe laser wavelength was at 282 nm in order to detect OH via excitation of the $A^2\Sigma^+$-$X^2\Pi_i$ (1,0) transition. 282 nm was generated by the same Nd:YAG laser (532 nm output), but operating with Rhodamine 6G dye, producing 564 nm, with frequency doubling in KDP crystal then used to generate ~1.5 mJ $pulse^{-1}$ at 282 nm. As well as the free-radical under kinetic observation, OH can also be used as the thermometer to measure the rotational temperature within the flow.[29] The probe laser could either be co-propagated with the photolysis beam along the axis of the gas flow, using a dielectric mirror to combine the two beams outside the chamber, or directed perpendicularly to the pholysis laser beam with the crossing-point within the imaging region of the fluorescence collection optics, as shown in Figure 1(b). For the crossed-laser beam arrangement, the probe laser entered and exited the main chamber via quartz windows held at Brewster's angle (on flanges 3 and 4, Figure 1(a)) to minimise scattered light. Both arrangements were used, as the overlap region of the gas-flow/photolysis laser/probe laser/fluorescence imaging volume is different in the two cases, allowing checks to be made on the homogeneity of the gas flow. The results were found to be independent of the arrangement used. The diameter of the 282 nm probe laser beam was ~ 2 mm at the fluorescence imaging region, and if

progagating along the axis of the flow, this is much smaller than the nozzle throat in order to minimise scattered light. For either arrangement the relative probe laser pulse energy was recorded by a UV photodiode using a quartz plate before the chamber to split off a small fraction of the beam, for subsequent normalisation of the LIF signal. The control of the timing of the firing of the lasers with repect to each other and to the firing of the pulsed-valves was controlled by a delay generator (Berkeley Nucleonics Corporation 555). The stepping of the dye-laser grating and doubling crystal and hence the wavelength of the probe laser and optimum phase matching angle was controlled by a computer using LabVIEW^{TM} (v. 6.1., National Instruments).

Fluorescence collection optics

The fluorescence collection axis is mutually perpendicular to the gas flow and laser-propagation axes, and in order to maximise the solid angle of collection of the laser-induced fluorescence, the fluorescence collection optics are positioned inside the chamber on two stainless-steel rails that pass across the axis of the chamber between two of the flanges (5 and 6), as shown in Figure 1(b). The mounts holding these optics can be translated perpendicularly to the gas flow on these rails for optimal performance. A quartz plano-convex lens (Crystan, diameter 50 mm, focal length 100 mm) is used to collimate the fluorescence, and the solid-angle of collection is increased through the use of a curved mirror placed on the opposite side of the imaging volume. The collimated fluorescence is then focussed by a second quartz plano-convex lens (identical to above) through a quartz window onto the photocathode of a photomultipler (PMT, Thorn EMI 9813QB). Following excitation of NO in the A-X (0,0) band at 226 nm, fluorescence is emitted over a range of wavelengths in the (0,v″) bands, and to discriminate against scattered light a band-pass filter (UG-5) was placed in front of the PMT to transmit off-resonance fluorescence at wavelenghts above 240 nm. Following excitation of OH in the A-X (1,0) band at 282 nm, off-resonance fluorescence is collected by an interference filter (Barr Associates Inc., 50 mm diameter, λ_{centre}=308.5 nm, FWHM = 5 nm), from the (1,1) band and also the (0,0) band, with the v′=0 level populated via collision-induced vibrational energy transfer.

Signal processing and data acquisition

LabVIEW^{TM} (v. 6.1., National Instruments) was used to control all aspects of signal capture, recording and processing, as well as the setting of the timing delays for the lasers and pulsed valves, and movement of the stepper motors. The outputs from the capacitance manometers and differential pressure transducers (for impact pressure measurements and pre expansion reservoir pressure measurement) were recorded by an A/D card (Measurement Computing USB-PMD1208LS) using the 12 bit differential analogue inputs. The output from the PMT was analysed in analogue mode. The OH fluorescence decay was captured by a digital oscilloscope (LeCroy Waverunner LT 264, 500 MHz, 8 bit vertical resolution), and the fluorescence signal integrated on a shot-by-shot basis between two pre-chosen time-points on the decay, and then averaged over a given number of laser shots. The output of the photodiodes to measure photolysis and probe laser pulse eneriges were processed by a simple *RC* circuit and sent to an oscilloscope for integration and recorded by the PC, for subsequent point-by-point normalisation of the LIF signal. The temporal decay of OH was obtained by changing the delay between the firing of the photolysis and probe lasers.

Results and discussion

Charaterisation of the pulsed Laval supersonic expansion

Two Laval nozzles designed for N_2 carrier gas were used in this work, whose design Mach numbers and flow temperatures were T = 106 K, M = 3 and T = 71 K, M = 4, both for a design gas density of $\rho = 5\times10^{16}$ molecule cm^{-3}. Both nozzles were fabricated using a computer numerical control (CNC) lathe. Further details of these nozzles can be found in Table 1. However, even though the shape of the nozzle is very close to that specified by the iterative computer code and used by the CNC lathe, it is very difficult to achieve the exact collimating background pressure, and also there are assumptions, for example regarding boundary conditions, in the underlying equations used by the code, which break down and lead to a slightly different Mach number. The design value, and the actual value of M, obtained by measurement of P_i/P_o and equation (E2), were found to be different, and prior to their use for kinetic studies it is necessary to characterise each nozzle in detail, measuring how each of these parameters varies in the flow with axial distance from the exit plane of the nozzle and radial distance from the centre. It is important to establish whether there are significant fluctuations or gradients of these parameters along or across the gas flow, which may aid the positioning and spatial overlap of the gas and laser pulses, or within the temporal envelope of the gas pulse. As components will age by repeated use, for example the magnetic poppits within the pulsed valves, whose wear changes the flow rate into the reservoir, it is necessary to periodically characterise the expansion. We have characterised the nozzles using a combination of dynamic impact pressure measurements and rotationally-resolved electronic spectroscopy.

Impact pressure measurements

The differential transducers, which are not calibrated by the manufacturer, were calibrated with reference to a known pressure difference as measured by two capacitance manometers (Leybold). Vacuum was used as the lower pressure and the transducers were calibrated up to their full pressure range.

The temporal evolution of the stagnation pressure (P_o) and the impact (dynamic) flow pressure (P_i) were recorded by two differential pressure transducers mounted in the reservoir and main chamber, respectively, with the values mathematically linked via equation (E2). The pressure transducers sampled the flow through a 1.5 mm diameter hole in its 6.5 mm diameter face. The reservoir/Laval nozzle assembly was translated in increments of 1 cm in order to vary the distance of the nozzle exit plane from the pressure transducer from 0 – 25 cm. Interference in the transducer output from the line-supply at 50 Hz was reduced by using a battery to power it, and a low-pass filter was used to reduce high-frequency noise, but without any alteration in the temporal profile. Figure 2 shows the temporal profile of the impact pressure of the gas pulse when the pressure transducer is positioned 20 cm from the Mach 3 nozzle, demonstrating a sharp rise and fall in pressure, and a pulse width of ~ 12 ms during which the impact pressure is reasonably constant. The stagnation pressure within the reservoir is also shown and demonstrates a similar temporal profile.

The stagnation pressure P_o in the reservoir and the dynamic impact pressure P_i in the flow was obtained from the difference between the calibrated transducer voltages during the gas pulse and the background voltage in between pulses. The value of P_i was measured for a variety of locations, and using equation (E2) could be used to determine the Mach number, *M*, from which the flow temperature, pressure and density at that location could be calculated using equations (E3), (E4) and (E5), respectively. Figure 3 shows how the temperature varies with axial distance 0 – 30 cm from the output plane of the Mach 3 nozzle as measured by a pressure transducer held in the flow, and positioned at the fluorescence imaging point, and aligned with the centre of the nozzle using an alignment laser. When averaged over all the measurements in the flow, the Mach number was calculated to be M=(3.5 ± 0.1). The parameters calculated from *M* averaged in the flow for 0 - 25 cm are summarised in Table 1, together with those for the lower temperature nozzle used in this work.

Figure 3 shows there are fluctuations in the temperature within the flow as one moves away from the nozzle. Such fluctuations are observed in all other Laval nozzle systems. The uniformity of the flow was optimised by changing the chamber pressure, which ideally should be the same as the pressure calculated in equation (E4). The oscillations cannot be attributed to any external factors, such as fluctuations in ballast or chamber pressures, or in the pulsed valves. The experimental variables of gas flow-rate, ballast tank pressure, reservoir pressure and chamber pressure were optimised via settings applied to mass flow controllers, valve pulse lengths and the throttling of the pumps to give the most stable flow. It was never possible to completely eliminate the oscillations, which were more or less evident depending on the individual nozzle used. Flowing additional gas into the chamber (the slip gas) via an additional port to adjust the cell pressure had little or no effect on the stability of the flow, probably because the pumps are providing a background pressure close to that required for a stable flow. The oscillations may indicate the presence of oblique shocks at the nozzle exit rather than a normal shock wave, which is perpendicular to the gas flow. Further discussion of this point can be found in ref.[24] Beyond about 20 cm from the Mach 3 nozzle, the impact pressure, and hence the Mach number and temperature, appear to drop off, being indicative of the failure of the Rayleigh formula when the Mach number drops significantly at the end of the relatively uniform flow. The rotational temperatures presented below show that the temperatures do not drop signifcantly at this point. The range of gas densities and temperatures within the flow have implications for the kinetic measurements described below, and must be taken into account in the calculation of uncertainties.

As the fluorescence is imaged from a finite volume within the gas flow it is important also to establish any variation in the temperature and density as a function of the radial distance from the centre. Figure 4 shows the axial and radial distribution of the impact pressure P_i for the Mach 3 nozzle, from which it can be seen that there are only ~ 5 - 10 mm of stable flow in the transverse direction, but that the flow is centrally located within the chamber. Careful alignment of the photolysis and probe laser beams with the gas flow is therefore crucial, and was facilitated through the use of irises.

Rotational temperature measurements

The measurement of the dynamic impact pressure provides an indirect method to obtain the Mach number, *M*, and hence the translational temperature, *T*, but as it is such a critical parameter for kinetic studies an independent measurement is highly desirable. At a density of 5×10^{16} molecule cm^{-3} and 90 K it is expected that translational and rotational degrees of freedom are rapidly equilibrated, as has been observed in previous studies of such jets.[21, 23, 24] We have obtained the rotational temperature by using LIF excitation spectra of either NO or OH to measure the rotational populations of several rotational levels and fitting a Boltzmann function to the data, or by a best fit to simulated spectra. The LIF signal excited from a ground-state with quantum number J″, and normalised for changes in laser power, is given by:

$$S_{J''} = C\, B_{J''}\, \phi_{J'}\, g_{J''} \exp(-E_{J''}/k_B T) \qquad \text{(E6)}$$

where the constant C contains experimental parameters that do not depend upon J, for example the total OH or NO concentration, solid angle of fluorescence collection, the transmission of optical components, PMT quantum efficiency etc., $B_{J''}$ is the Einstein B coefficient, $\phi_{J'}$ is the fluorescence quantum yield of the electronically excited state, and $g_{J''}\exp(-E_{J''}/k_BT)$ is the Boltzmann population of the rotational level with energy $E_{J''}$ ($g_{J''}$ is the degeneracy). Care must be taken to ensure that the value of $\phi_{J'}$ does not change significantly with J′ (and hence J″), for example due to changes in the rate coefficient for collisional quenching of the excited state and the range of fluorescence wavelengths emitted, both of which will vary with J′. However, at the low temperarures within the flow the range of J″ is relatively small, and these effects can be mitigated using a short fluorescence integration gate and ensuring a sufficiently wide range of fluorescence wavelengths reach the detector.[29] Laser excitation spectra were measured over a range of laser pulse energies, controlled either by the use of neutral density filters or using a quartz flat instead of a mirror or prism to direct the laser into the Laval chamber, to ensure there is no optical saturation for any of the rotational transitions. The concentration of NO and OH is low enough that self-absorption of fluorescence, which may be J″ dependent, is not significant. Assuming that $\phi_{J'}$ is constant with J, the natural logrithmic form of equation (E6) is given by:

$$\ln\left(\frac{S_{J''}}{B_{J''}g_{J''}}\right) = D - \frac{E_{J''}}{k_B T} \qquad \text{(E7)}$$

where D is a constant, and hence a plot of the LHS of (E7) versus $E_{J''}$ yields a gradient of $-1/k_BT$.

Figure 5(a) shows a laser excitation spectrum for the Mach 3 nozzle with NO present at 0.01% in the N_2 flow, together with a Boltzmann plot, at a position 20 cm from the nozzle and ~ 4 ms into the pulse. Peak areas were determined using peak-fitting software (PeakFit v4.12, Seasolve Software Inc.). At the laser spectral resolution used (~0.5 cm^{-1}), the R_1 line and its R_{21} satellite, which emanate from the same ground state quantum state, are not resolved, and thus the sum of Einstein B coefficients was used in the Boltzmann analysis. Rotational energies were calculated using spectroscopic data from Paul,[30] and Einstein B absorption coefficients taken from LIFBASE.[31] The gradient (= $-1/k_BT$) of Figure 5(b) yields a temperature of 84 ± 4 K. Rotational temperatures obtained at other distances from the Mach 3 nozzle (but at the same time within the pulse) are overlaid in Figure 3 together with the translational temperatures obtained from impact pressure

measurements for this nozzle. The average NO rotational temperature over the range 0 – 20 cm is 84 ± 5 K (1σ) which agrees well with the corresponding value of 86 ± 3 K (1σ) obtained from a much larger number (20) of impact pressure measurements. At 25 cm from the nozzle the rotational temperature is significantly higher than at 20 cm, when the uniform flow begins to break up, whereas the temperature from impact pressure decreases due to the breakdown of the Rayleigh equation.

The length of the gas pulse (~12 ms, Figure 2) is much longer than the time taken for the gas to flow from the nozzle to the fluorescence collection region, which is ~ 300 μs for the Mach 3 flow. Hence there is a considerable time window in which to fire the photolysis laser and generate OH radicals, and monitor the kinetic decay over ~ 300 μs. By changing the delay of the firing of the NO probe laser relative to the opening of the pulsed valves, it is possible to detect NO at various times within the gas pulse, and by performing an excitation scan, the corresponding temperature can be measured, as shown in Figure 2. Within the main portion of the pulse there is some variation in the temperature (~± 10 K), similar to that observed in other pulsed Laval systems,[32] but towards the end of the gas pulse the rotational temperature rose significantly to ~ 175 K, as the stable flow begins to break up.

A smaller number of temperature measurements were made from laser excitation spectra of OH, with OH generated from the photolysis of *t*-butyl hydroperoxide. The considerably larger rotational constant for OH compared with NO gives a maximum population at 86 K for J″=1.5, making OH less ideal for rotational temperature measurements, but the high signal-to-noise ratio enabled transitions from up to J″=4.5 to be observed. Care was taken to ensure that there was a sufficiently long delay (> 50 μs) after photolytic production of OH for rotational thermalisation of a nascent distribution to be complete. The computer program LIFBASE [31] was also used to calculate the laser-excitation spectra of OH and NO in the A-X (1,0) and (0,0) bands, respectively, at the experimental spectral resolution. The input temperatures which gave the optimal fit to experiment were very close to those obtained using the Boltzmann analysis for the Mach 3 nozzle. At a flow distance of 20 cm, and for OH excited at the same time within the gas pulse, rotational temperatures between 80-90 K were obtained.

The good agreement between various methods for the measurement of temperature gives confidence that the temperature profile along and across the flow, and also within the temporal envelope of the pulse itself, is well characterised and understood. Similar nozzle characterisations were performed for the Mach 4 nozzle, but temperature profiles were only determined using impact pressure measurements.

Measurement of rate coefficients

For a given Mach number within the flow, the distance between the exit-plane of the Laval nozzle and the fluorescence imaging volume defines the maximum time available for detection of OH during a kinetic decay. For the Mach 3 nozzle, 20 cm represents a conservative estimate of the limit of stable flow, and was used for the kinetics experiments, and for a gas flow velocity of 663 ± 30 ms^{-1}, corresponds to a maximum reaction time of ~ 300 μs. One criterion for being able to measure a rate coefficient accurately is the requirement to measure approximately one half-life of the decay of the free-radical under study, which in turn corresponds to a pseudo-first-order rate coefficient of $k' \sim 2280\ s^{-1}$. Unless the ratio of heat capacities, γ, for the excess reagent is the same as for the carrier gas, N_2, then a rule of thumb is that the maximum mixing ratio of the excess reagent cannot exceed ~ 1% that of N_2 without disturbing the conditions of the flow, which for the Mach 3 nozzle used here corresponds to a excess reagent density of $\sim 5 \times 10^{14}$ molecule cm^{-3}. Therefore a minimum bimolecular rate coefficient of $k_{bi} \sim 4.5 \times 10^{-12}$ cm^3 $molecule^{-1}$ s^{-1} is required. In reality, the lowest determinable value of k_{bi} depends on the ability to distinguish the rate of OH removal by the excess reagent in the reaction time available compared with losses by other routes (e.g. diffusion or reaction with the precursor), which manifest themselves in the magnitude of the intercept of the second order plot of k' versus concentration of excess reagent, and hence will depend on the signal-to-noise of the system.

Photolysis of *t*-butyl hydro-peroxide ($(CH_3)_3COOH$, referred to here as *t*-BuOOH) at 248 nm was chosen as the souce of OH for several reasons. It is available as a 70% solution in water (compared to 50% for H_2O_2), and importantly, it has a vapour pressure (23 Torr at 21°C, data supplied by manufacturer) which is considerably higher than water vapour (18.36 Torr at 20°C), whereas H_2O_2 has a vapour pressure (6 Torr) that is lower. The amount of water vapour in the flow is therefore low (< 10%), minmising any possible effects it may have, for example, as a catalyst as observed in recent studies of radical-molecule reactions using a pulsed Laval nozzle.[26] *t*-BuOOH was entrained into the N_2 flow using a air-tight glass bubbler (held at 1370 Torr), and following further dilution in N_2 was estimated to be at a mixing ratio of ~ 0.05 % entering the reservoir region. *t*-BuOOH is readily and cheaply available, and is relatively stable compared with other subsituted peroxides, for example CH_3OOH, and can be stored without decomposition in the glass bubbler for > 1 month. It is known to undergo some decompositon on metal surfaces,[33] but more slowly than for H_2O_2.[33] Compared with production of OH from reactions of $O(^1D)$ with hydrocarbons, photolysis of *t*-BuOOH is a clean and more straighforward source of OH, and is considerably less corrosive than other photolytic precursors, for example nitric acid.

The initial concentration of OH was estimated as 1×10^{11} molecule cm^{-3} from knowledge of the excimer laser fluence in the chamber at 248 nm and the absorption cross-section of *t*-BuOOH at 248 nm, which is in the long-wavelength tail of its UV absorption continuum.[34]

In all experiments the pulse repetition frequency of both lasers and the nozzle valves was 5 Hz. Absorption at 248 nm excites *t*-BuOOH to the repulsive $\tilde{A}^1A$ state via a $\sigma^* \leftarrow n$ transition localised in the O-O bond, and is followed by prompt dissociation to generate OH exclusively in the $X^2\Pi$ v"=0 level[34, 35], avoiding any complications due to vibrational cascade from higher levels into v"=0 during the kinetic decay. There is some rotational excitation, mostly originating from torsional forces about the O-O bond during the dissociation, but this will be rapidly thermalised at the densities used here.

Measurement of rate coefficients for $OH+(CH_3)_3COOH$

The kinetics of the reaction of OH with H_2O_2 have been well studied, with a recent measurement by Vakhtin et al. yielding a rate coefficient of 1.78×10^{-12} cm^3 $molecule^{-1}$ s^{-1} at 296 K, increasing significantly to 1.99×10^{-11} cm^3 $molecule^{-1}$

s^{-1} at 96 K measured using a pulsed Laval nozzle.[36] For OH+CH_3OOH, there have only been three kinetic studies,[37-39] including a room temperature determination of the rate coefficient of $(9.0 \pm 0.2) \times 10^{-12}$ cm^3 $molecule^{-1}$ s^{-1} in this laboratory.[39] Only one measurement in 1978 has been made of the rate coefficient for the reaction of OH with *t*-BuOOH, giving a value of $(3.0 \pm 0.8) \times 10^{-12}$ cm^3 $molecule^{-1}$ s^{-1} at 298 K,[40] between the values for CH_3OOH and H_2O_2. The reaction of OH with H_2O_2 has a strong inverse temperature dependence,[36] on account of the stability of the OH-H_2O_2 intermediate, and it is thus expected that the reaction between OH and *t*-BuOOH follows the same trend.

The reaction between OH and *t*-BuOOH was studied in the absence of other reagents using the Mach 3 nozzle at 86±4 K. In order to vary [*t*-BuOOH] a cylinder of 0.15% *t*-BuOOH in N_2 was prepared, and flowed through a flow controller, followed by further dilution with a known flow of N_2. The decay of OH was measured for 300 μs (time to flow 20 cm) following the excimer laser for [*t*-BuOOH] in the range 0.004-0.15% at a constant flow rate of 1565 sccm delivered to the reservoir. The temporal evolution of the OH LIF signal under pseudo-first-order conditions of [*t*-BuOOH] >> [OH], is given by:

$$S_t = S_{t=0} \exp(-k't) + I_{offset} \quad \text{(E8)}$$

where k' is the pseudo-first-order rate coefficient for OH loss and I_{offset} is any instrumental offset. For all kinetic studies, the OH radical was detected using the $Q_1(J''=1.5)$ transition at 281.9 nm. As *t*-BuOOH is the OH precursor, then $S_{t=0}$ is proportional to [*t*-BuOOH]. Equation (E8) was fitted to the OH profile, S_t, to obtain k', which is given by:

$$k' = k_1[t\text{-BuOOH}] + k_d \quad \text{(E9)}$$

where k_1 is the rate coefficient for OH+ *t*-BuOOH and k_d is the first-order rate coefficient for diffusive and other first-order losses of OH. k_1 was obtained from linear-least squares gradient of a graph of k' against [*t*-BuOOH], over the range 3.1 - 47 × 10^{12} molecule cm^{-3}, which yielded $k_1 = (7.8 \pm 2.5) \times 10^{-11}$ cm^3 $molecule^{-1}$ s^{-1} at 86±4 K, with an intercept of $k_d \sim 2500$ s^{-1}. At [OH] ~ 10^{11} molecule cm^{-3}, OH loss by its self-reaction can be neglected. Ivanov et al. determined the diffusion coefficient of OH in air at 298 K to be $D_{diff,OH} = 163 \pm 20$ cm^2 Torr s^{-1} [41] and using:

$$\frac{D_{diff,OH}(p_1,T_1)}{D_{diff,OH}(p,T)} = \frac{p}{p_1}\left(\frac{T_1}{T}\right)^{1.75} \quad \text{(E10)}$$

we estimate $D_{diff,OH} = 32 \pm 4$ cm^2 Torr s^{-1} within the cold flow. Using the value of k_d above this corresponds to an average distance moved of ~ 2 mm, which is consistent with the photolysis and probe laser beam radii of ~4 and ~2 mm, respectively.

The value of k_1 is subject to some uncertainty, as [*t*-BuOOH] was not measured directly, e.g. by absorption spectroscopy, rather calculated by knowledge of the vapour pressure of *t*-BuOOH used to make up the cylinder, and the gas flow rates, and there may have been some decomposition on the cylinder walls. However, the accuracy of k_1 is not crucial to the remainder of this paper, but the value at 86 K is ~ 26 times larger than at 299 K,[40] consistent with the observed trend (factor of ~8 increase) in the corresponding rate coefficient for H_2O_2 on lowering the temperature from 296 to 96 K observed by Vakhtin et al.[36] Clearly, similar long-range attractive forces are important for the reactions of OH with H_2O_2 and *t*-BuOOH.

Measurement of rate coefficients for OH+C_2H_4

In order to maintain the same density throughout an experiment, the total gas flow was kept constant, with the N_2 carrier gas flow reduced accordingly as the ethene flow was increased. The flow of ethene was varied from 0-1 % of the total flow, with the precursor kept constant at ~ 0.05 %, and N_2 making up the remainder.

In the presence of ethene, the OH decay rate, given by k', is given by:

$$k' = k_1[t\text{-BuOOH}] + k_d + k_2[C_2H_4] \quad \text{(E11)}$$

where k_2 is the rate coefficient for the OH+C_2H_4 reaction. The nozzle exit-plane was placed 20 cm from the fluorescence imaging volume, and the excimer laser pulse fired ~6 ms into the gas pulse (shown on Figure 2). The LIF signal from OH was measured at 400 points between 0 – 300 μs, together with 20 points of background when the probe laser was fired before the excimer laser. For each delay the LIF signal was averaged over 2 laser shots, and in total 20 OH decays were averaged. Recording the decay fairly fast and co-adding a number of decays minimises the effects of any slow drift in the laser wavelength. At the lowest [C_2H_4] the OH signal did not completely decay to the background within 300 μs. If the OH signal was recorded beyond this time it was seen to increase dramatically, once gas that was still within the reservoir at the time of photolysis reaches the fluorescence imaging volume. A typical temporal evolution of S_{OH} is displayed in Figure 6. The pretrigger points are used to obtain I_{offset}.

For each temperature, 69±3 and 86±4 K, the OH decays, S_{OH}, were recorded as a function of [C_2H_4] and k' obtained from a fit of equation (E8) to the data. Figure 7 shows k' plotted versus [C_2H_4] for each temperature, from which k_2 was obtained from the gradient of a fit of equation (E11) to the data, and Table 2 summarises the results and conditions used. The value of the intercept is dependent upon the nozzle used and precise alignment of the lasers, but for a typical value of ~ 4000 s^{-1}, has contributions from k_1[*t*-BuOOH] ~ 1500 s^{-1} (0.05% *t*-BuOOH and using k_1 determined above) and $k_d \sim 2500$ s^{-1}. In a smaller number of experiments, the Laval nozzle was positioned in a different axial position along the flow, and the OH temporal decay recorded at a smaller distance between the nozzle exit-plane and fluorescence imaging volume. In this case the maximum reaction time that can be studied is shorter. Experiments were also performed when the excimer photolysis laser was fired at a different time during the gas pulse. However, no systematic differences were found in the value of k' measured in any of these experiments.

The values of k_2 are seen to increase significantly with lowering temperature, consistent with the absence of a barrier to reaction, and with the Smith et al.[2] rule. However, there are very few measurements below room temperature with which to compare the current results. The potential energy surface for OH + C_2H_4 was recently calculated by Cleary et al.[27] using DFT-BH&HLYP/6-311+G(3df,2p) for geometries, zero point energy and intrinsic reaction coordinates, with energetics calculated at the CBS-APNO level (±2-4 kJ mol^{-1}). The calculations show a van der Waals complex at long range with

a zero-point well-depth of 7.7 kJ mol^{-1} relative to that of the reagents. The barrier for the decomposition of this complex to form the OH-C_2H_4 adduct is 3.7 kJ mol^{-1} below the reagent energy. Hence the reaction proceeds with no overall barrier, consistent with the negative temperature dependence observed down to 69 K.

Although in this work values of k_2 were only obtained at a single density of $[N_2]\sim4\times10^{16}$ molecule cm^{-3}, it is instructive to compare the measurements with master equation calculations of the pressure dependence recently published by Cleary et al.[27] utilising this potential surface. Cleary et al.[27] measured k_2 between 5 – 600 Torr and at temperatures between 200 - 400 K using FP-LIF in a cooled cell. The majority of experiments were performed in He and a more limited set in N_2 (at 300 K) as a third body. The helium data were used to extract the high-pressure rate coefficient k_∞ by fitting single-well Master Equation (ME) calculations to the data, yielding $k_\infty(T) = 5.01 \times 10^{-12} \exp(148/T)$ cm^3 $molecule^{-1}$ s^{-1}, a value which was also used for N_2. The ME calculations were then optimised, using the inverse Laplace transformation[42] to obtain microcanonical rate-cofficient $k(E)$ for dissociation of the C_2H_4-OH adduct from the measurements of k_∞, and fitting to the available observed pressure fall-off data in He and N_2. The average downward energy transfer parameter $\langle\Delta E\rangle_{down}$ for He and N_2 was treated as a variable parameter and for N_2 $\langle\Delta E\rangle_{down}$ was found to be 220 cm^{-1} from the best fit to the 300 K data. In addition, these ME calculations were compared with low-temperature determinations of k_2 in N_2 at 96 K, 110 K and 165 K, which were measured in a pulsed Laval nozzle by Vakhtin et al.[43] It was found that the calculated k_2 significantly underestimated the experimental observations of Vakhtin,[43] as shown in Figure 8(a), and it was concluded that further measurements of k_2 at low temperatures for different pressures were needed.[27] Finally, parameterisations of the ME expressions for k_2 were obtained by fitting them to a Troe expression[44] to determine the low-pressure rate coefficient, k_0, and a temperature independent fall-off parameter F_{cent}, given by:

$$k_2 = \frac{k_0[M]}{k_\infty + k_0[M]}F \quad \text{where} \quad \log F = \frac{\log F_{cent}}{1+\left[\log\left(\frac{k_0[M]}{k_\infty}\right)\right]^2} \qquad \text{(E12)}$$

and

$$k_0 = A_0\left(\frac{T}{300}\right)^{m}0 \qquad \text{(E13)}$$

which for N_2 yielded $A_0 = 2.47 \times 10^{-29}$ cm^6 $molecule^{-2}$ s^{-1} and $m_0 = -4.32$.

Figure 8(a) shows the pressure dependence of k_2 calculated using the parameterised Troe expressions obtained in Cleary et al.[27] for 69, 86, 69, 110 and 165 K, together with the measurements obtained from the pulsed Laval nozzle in this work at 69 and 86 K and the values of k_2 obtained by Vakhtin et al. at 96, 110 and 165 K.[43] Over the range of densities studied experimentally, Figure 8(a) demonstrates that k_2 is significantly below its high-pressure limit at 165 K but for $T \leq 100$ K, the reaction is within 15% of its high-pressure limit above $[N_2] = 5 \times10^{16}$ molecule cm^{-3}. The experimental data of Vakhtin et al. [43] are significantly underestimated by the Troe expression used by Cleary et al.[27], as previously noted, but the data from this present study are only slightly overestimated by this expression.

Greenwald et al.[3] also used a ME approach to calculate k_2, but used both an outer (tight) and inner (loose) transition state on the potential energy surface, with the pre-reaction van der Waals complex, bound by long-range attractive forces, lying between the two. A variational two transition state model, coupled with a two-dimensional master equation (energy and angular momentum) was used to calculate the temperature dependence of k_2. The calculated data for k_∞ from Greenwald et al.[3] was used in a ME to fit the available literature values for k_2 (the data of Cleary et al.[27] were not available), and with modest changes to k_∞ Greenwald et al.[3] were able to obtain a good fit to the experimental data, which included the low temperature data of Vakhtin et al.[43] The fall-off data of Greenwald et al.[3] were in turn fitted using a Troe formalism by Cleary et al.[27], and in Figure 8(b) the Troe fits are compared to the experimental values of k_2 obtained in this study and by Vakhtin et al.[43] From Figure 8(b) it is evident that the data obtained in this study are significantly overestimated, especially at 69 K, where there is a factor of three difference. The data of Vakhtin et al.[43] are well described by the Troe fits to the Greenwald ME calculations, but this is to be expected as the ME derived values of k_2^∞ were adjusted to fit this very data set. A significant reduction of k_2^∞ would be required in order to agree with the present data.

The theoretical approach used by Greenwald to determine k_2^∞ relies on the calculation of an accurate *ab initio* potential energy surface (PES), which is difficult for a barrierless reaction, and the details of the PES generally require adjustment in order to match experimental kinetic data. Cleary et al. [27] adopted a more pragmatic approach of measuring k_2 over a range of temperature and pressure, and using an Inverse Laplace Transform / Master Equation approach to calculate k_2^∞ over the experimental range of temperatures, which were then fitted to a temperature expression of the form $k_2^\infty = A^\infty\times(T/300)^{n\infty}$, in order to extrapolate. The values for k_2 measured in the present study are in fair agreement with those calculated using the single-well ME treatment described by Cleary et al.[27] (figure 8(a)), but are not consistent with those determined by Vakhtin et al.[43], which were used to optimise the Greenwald et al.[3] two-well master equation calculation. The reason for the discrepancy between the two experimental studies is unknown.

Measurement of rate coefficients for OH+C_2H_2

Only one determination of the rate coefficient for OH+C_2H_2 (ethyne) was made at 69 K with the Mach 4 nozzle for a gas density of 3.66×10^{16} molecule cm^{-3}. The gas mixture consisted of 0.05 % *t*-BuOOH, 0-1% ethyne and the remainder N_2. No significant observable change in k' was observed for $[C_2H_2]$ in the range 0 - 2.75×10^{14} molecule cm^{-3}, from which an upper limit for the rate coefficient of $k_3 < 1\times10^{-13}$ cm^3 $molecule^{-1}s^{-1}$ was obtained.

Until very recently, the only measurement of k_3 below room temperature was that of Michael et al.[45]. A very recent study from Leeds (McKee et al.[46]) measured the temperature and pressure dependence of the rate coefficient in He over the range 210 – 373 K and 5- 760 Torr, and also in N_2 and SF_6 at room temperature. A full summary of previous determinations and calculations of k_3 in the literature is given in McKee et al.[46] The results yielded the following expression for $k_{3,\infty}$:

$$k_{3,\infty}(T) = 7.3\times10^{-12}\exp(-5300/RT)\ cm^3\ molecule^{-1}\ s^{-1} \qquad \text{(E14)}$$

which although outside of the range of its intended usage yields $k_{3,\infty}$ (69 K) = 7.1 × 10^{-16} cm^3 $molecule^{-1}s^{-1}$. The presence of a small energy barrier to the formation of the OH-C_2H_2 adduct was confirmed by McKee et al.[46] from experiments and using *ab initio* calculations at the DFT-B3LYP/6-311+G(3df,2p) level, obtaining E_a = 6.5 kJ mol^{-1}, similar to an earlier calculation of 4.6 kJ mol^{-1}.[47]

A weakly-bound T-shaped OH-C_2H_2 van der Waals complex has been observed within a supersonic free-jet expansion for which the binding energy was measured to be 11.4 kJ mol^{-1},[48] and confirmed by ab initio calculations.[48] The van der Waals complex is likely to be formed without a activation barrier, and at the low temperatures of the pulsed Laval expansion (down to 69 K in the present work) formation and stabilisation of the complex might be expected to lead to a measurable loss of OH radicals. However, this was not observed, and so it is concluded that under our conditions the complex is not formed to a great extent. Lower temperatures (as produced in a free-jet expansion[48]) or consierably higher densities may be required to stabilise the complex and enable it to be inferred via loss of signal from the OH reagent.

Measurement of rate coefficients for OH+C_3H_4

For the reaction of OH with C_3H_4 (propyne or methyl acetylene), measurements were made at 69 K (Mach 4 nozzle), 86 K (Mach 3 nozzle) and 299 K (the latter temperature measured using a thermocouple with the Laval nozzle removed from the chamber) at a gas density of ~3.7×10^{16} molecule cm^{-3}. The gas mixture consisted of 0.05 % *t*-BuOOH, 0-1 % C_3H_4 and the remainder N_2. Figure 9 shows the values of k' obtained as a function of [C_3H_4] for these three temperatures, from which the gradients yield k_4, and the results are summarised in Table 3.

These results are the first obtained below 253 K, and overall k_4 shows a weak temperature dependence, significantly less than for ethene, but again, consistent with the rule of Smith et al.[2] Previously, this reaction has been studied by Boodaghians et al.[49] who observed a weak temperature dependence between between 253-343 K using the discharge-flow resonance fluorescence method, but did not observe any significant pressure dependence over the limited range studied (1.7 - 6.4 Torr). The present work has determined k_4(299 K) = (3.11 ± 0.09) × 10^{-12} cm^3 $molecule^{-1}s^{-1}$ at a pressure of ~ 1 Torr and is in good agreement with the value of k_4 = (3.05 ± 0.14) × 10^{-12} cm^3 $molecule^{-1}s^{-1}$, obtained by Boodaghians et al.[49] around 1.7 - 6 Torr. However, Atkinson and Aschmann,[50] and Hatakeyama et al.[51] determined k_4 at room temperature and atmospheric pressure, and observed a value approximately twice that of Boodaghians et al.[49], suggesting that both the study of Boodaghians et al.[49] and of our own are in the fall-off region. The very high value for k_4 obtained by Bradley et al.[52] in 1973 using ESR at 2.5 Torr appears to be inconsistent with our and all previous data.

If the reaction reaches its room temperature, high pressure limit close to atmospheric pressure, and k_4^∞ is ~ 6 × 10^{-12} cm^3 $molecule^{-1}s^{-1}$, with only a slight negative temperature dependence, this implies there is little or no barrier to reaction, similar to the OH/ethene system. The additional methyl group in propyne compared with ethene would be expected to give a more strongly bound van der Waals complex, but the absence of any barrier for its decomposition to the strongly bound OH-C_3H_4 adduct suggests a very short lifetime.

Hatakeyama et al.[51] proposed a reaction mechanism involving selective electrophilic attack of OH onto the terminal carbon of the C≡C bond, and in the presence of O_2 and NO_x, chamber FTIR end-product studies confirmed the presence of $CH_3C(O)C(O)H$ (methylglyoxal) and $CH_3C(O)O_2NO_2$ (peroxyacetyl nitrate), but no formation of CH_3COOH (acetic acid), which would have resulted from OH initially attacking the central C atom. These experiments were confirmed by using OD as a reagent. The pressure dependence can be explained by third-body stabilisation of the initially formed $CH_3C{\equiv}C(H)OH$ adduct. However, this mechanism was not supported by recent experiments by Yeung et al.[53] who used chemical ionisation mass spectrometry to show that at 298 K and 100 Torr the major products were methyl glyoxal and acetic acid, with some evidence for formic acid, suggesting OH attack at the central C atom, whose electron density is increased by the inductive effect of the neighbouring CH_3 group. Yeung et al.[53] also calculated the potential energy surface and transition state energies using a modified G2MS method.

A study of the reaction of OH with benzene and toluene

A mixture of 1.5 % benzene in N_2 was made up in a gas cylinder at a total pressure of ~ 6000 Torr. For the Mach 3 nozzle at 86 K, OH decays in the presence of the *t*-BuOOH precursor and N_2 only showed the normal single-exponential behaviour, but in the presence of the intended reagent benzene, the OH signal at *t*=0 increased by about a factor of 6 and the OH temporal profile showed a *growth*, lasting for ~250 μs, followed by a slight decay prior to the end of usable 300 μs in the gas flow. One hypothesis is that OH($X^2\Pi$, v″>0) is being formed from the 248 nm photoylsis of binary or larger complexes of the precursor and benzene that form during the supersonic expansion, followed by vibrational cascade into the laser-excited v″=0 level. However, detecting OH via the $A^2\Sigma^+$-$X^2\Pi_i$ (2,1) band near 288 nm yielded no observable LIF signal from v′=1, and appears to rule out this hypothesis. A similar growth of OH was observed at room temperature without the Laval nozzle implying that photolysis of clusters is not the cause.

Bohn and Zetzsch[54] studied the reaction of the OH-benzne adduct with O_2 at 297 K and atmospheric pressure, using the 248 nm photolysis of H_2O_2 as the OH source. Similar to this work, they observed that the OH LIF signal increased by a factor of 6 before levelling off as the concentration of benzene increased. It was proposed that benzene is excited at 248 nm to the first electronically excitged S_1 state ($^1B_{2u}$), followed by rapid intersystem crossing to the much longer-lived triplet T_1 state ($^3B_{1u}$), which collisionsally sensitizes the decomposition of H_2O_2 to give two OH molecules. When O_2 was added to their system, the effect was suppressed, consistent with the rapid quenching of the benzene T_1 state by O_2. The analogous triplet benzene sensitised decomposition of *t*-BuOOH could therefore be a source of OH. Addition of ~0.2 Torr O_2 (20% of the flow) did not affect the OH profile, either at 86 K or at room temperature. The rate coefficient for the quenching of benzene T_1 has previously been measured at room temperature by Morikawa and Cvetanovic[55] to be 2.1 × 10^{-11} cm^3 $molecule^{-1}s^{-1}$, consistent with the work of Bohn and Zetzsch[54] where the addition of 30 Torr O_2 was sufficient to supress the triplet. It is unlikely that the quenching of triplet benzene by O_2 has an activation barrier. The results of the present study therfore suggest that 0.2 Torr of added O_2 is not sufficient to significantly quench the triplet state of benzene, and hence affect the OH temporal profile.

The experiments were repeated with toluene, with toluene-N_2 mixtures again made up in a cylinder at ~ 6000 Torr. Once again a growth in the OH signal was observed over the same timescale as seen for benzene, which was not affected by the addition of O_2, suggesting that the same mechanism is operating for both benzene and toluene. These experiments provide some evidence for the aromatic sensitised decomposition of the peroxide generating OH, with the addition of 0.2 Torr O_2 not being sufficient to significantly quench the triplet state of the aromatic.

Conclusions

Rate coefficients have been determined for the reactions of OH with *t*-butyl-hydroperoxide ($(CH_3)_3COOH$), ethene (C_2H_4), ethyne (HC≡CH) and propyne ($CH_3C{\equiv}CH$) at very low temperatures generated within a pulsed supersonic expansion from a recently constructed Laval nozzle apparatus. The temperature in the flow was determined axially and radially, and values obtained from impact pressure measurements agreed with spectroscopically determined rotational temperatures from OH and NO. For the unsaturated hydrocarbons the kinetics obey the Smith et al. [2] rule that reactions with IE-EA of less than ~ 9 eV, where IE is the ionisation energy of the unsaturated molecule, and EA is the electronic affinity of the free-radical, will be fast at low temperatures. For ethyne, only an upper limit for the rate coefficient could be measured at 69 K.. The result is consistent with the presence of a small (~ 5 kJ mol^{-1}) activation barrier for the formation of the chemically bound adduct, and consistent with Smith's rule, as IE-EA = 9.6 eV. For ethene, the rate coefficients k_2 at 69 and 86 K compare favourably with a Troe parameterised fit to single-well master equation calculations that had previously been optimised by comparison with measurements of k_2 reported at higher temperatures and pressures recorded in this laboratory.[27] However, the data are not consistent with another dual-well master equation calculation[3] optimised using another low-temperature pulsed Laval determination of k_2.[43] For propyne, no previous measurements below 253 K had been made, but the results show a modest negative temperature dependence of the rate coefficient. For benzene and toluene, the temporal profiles of OH were not those of a single exponential decay, rather a delayed production followed by a decay, which could not be analysed under the time available within the pulsed flow to determine meaningful rate coefficients.

Acknowledgements

The authors wish to thank the research groups of Professor Stephen Leone (University of California, Berkeley), Professors Ian Sims and Bertrand Rowe (Univerity of Rennes I) and Professor Mark Smith (University of Arizona, Tuscon), in particular Dr. Chris Mullen, for encouragement and assistance during the design and commissioning of the Leeds pulsed Laval system, and for the provision of detailed drawings and computer codes for the fabrication of the Laval nozzles themselves. Thanks are also given to Professor Ian Smith and Dr. Sven Kohler for helpful discussions, and to the University of Leeds, School of Chemistry mechanical and electronics workshops. The Laval nozzles were manufactured by the fabricating workshops of the School of Mechanical Engineering at the University of Leeds. We are also grateful to Professor Mike Pilling and Dr. Paul Seakins at Leeds for their support during this project. SET wishes to thank NERC for the provision of a postgraduate studentship.

Table and Figure Captions

Table 1.
Details of Laval nozzles used in this work. The carrier gas is N_2.

Table 2.

Summary of rate coefficient measurements for the OH + ethene reaction.

Table 3.

Summary of rate coefficient measurements for the OH + propyne reaction.

Figure 1.
(a) Three dimensional image of the pulsed Laval nozzle apparatus. Flanges 1 and 2 enable gas to be provided to the two pulsed valves as well passing electrical feed-throughs for control of stepper-motors and monitoring of pressures. The probe-laser beam enters and leaves the cell through Brewster angled windows mounted on Flanges 3 and 4. The fluorescence collection optics are mounted on rails held between Flanges 5 and 6.
(b) Schematic showing the details of the reservoir, Laval nozzle, supersonic flow and fluorescence collection system.

Figure 2.
Temporal evolution of the impact pressure in the supersonic flow with the differential pressure transducer positioned 20 cm downstream of the nozzle-exit plane, together with the profile of the pressure within the reservoir (stagnation) region. Also shown is the variation in the temperature throughout the gas pulse as measured by rotationally resolved laser-induced spectroscopy of NO, with the fluorescence collection axis positioned 20 cm downstream of the nozzle-exit plane. The uncertainty in the temperature is the 1σ error from a linear least squares fit of equation (E7) to rotational populations (see text for details). The increase in temperature as the flow breaks up at the end of the gas pulse can be seen. The arrow marks the position within the gas pulse at which the excimer laser was fired for kinetic studies, after which OH was monitored for 300 μs.

Figure 3.
Axial profile of temperature within the supersonic flow obtained by translating the Mach 3 Laval nozzle with respect to the pressure transducer, which was held at the fluorescence imaging point. Black diamonds (◆) indicate temperatures determined from rotationally resolved LIF spectra of NO, with the laser exciting NO ~ 4 ms after the beginning of the gas pulse. The average temperature along the flow was 84 ± 5 K (1σ). Grey squares (■) indicate temperatures calculated from impact pressure measurements using equation (E3), with an average value of 86 ± 3 K (1σ).

Figure 4.
Axial and radial variation of the impact pressure measured for the Mach 3, T = 86 K, [M] = 3.7×10^{-16} molecule cm^{-3} Laval nozzle.

Figure 5.
(a) Laser-excitation spectrum (normalised for laser power) in the Q_1 and R_1 branch region of the NO $A^2\Sigma^+$ (v′=0) ← $X^2\Pi$ (v″=0) transition. The spectral resolution was ~ 0.5 cm^{-1} and the laser was fired ~ 4 ms into the gas pulse generated by the Mach 3 nozzle, positioned 20 cm from the fluorescence imaging volume.
(b) A Boltzmann plot of logrithmic population versus rotational energy for the LIF spectrum shown in (a), together with the linear-least squares fit of equation (E7) to the data, the gradient of which yields a temperature of 83.5 ± 3.7 K (1σ).

Figure 6.
Typical OH temporal decay observed for the OH + ethene reaction studied with the Mach 3, 86 K, 3.7×10^{-16} molecule cm^{-3} density Laval nozzle, together with a least-squares fit of equation (E8) to the data. The rapid rise and initial part of the OH decay were not included in the fit, although the fit is plotted back to t = 0. [C_2H_4] = 3.7×10^{14} molecule cm^{-3}. The profile is the average of 20 decays each recorded with 2 laser shots per individual time point.

Figure 7.
Second order plots of the decay rate k' versus [C_2H_4] for T = 86 and 69 K. The individual error bars shown for each point incorporate the statistical error in the fitting of the exponential decay and the error in [C_2H_4] arising from density fluctuations in the supersonic gas flow, with the latter being the major contributor to the quoted uncertainty. The solid black lines are linear least-square fits of equation (E11) to the data, the gradients of which yield the values of k_2, and the solid grey lines represent the 95% confidence limits of the fitted line.

Figure 8.
(a) The solid lines are the Troe expressions for k_2 at 165, 110, 96, 86 and 69 K, using the expression from Cleary et al.[27] The open symbols are the data from Vakhtin et al.[43] at □(165 K), ○(110 K) and △(96 K). The filled symbols are the data for the present study: ■(86 K) and ● (69 K).
(b) The solid lines are the Troe expressions for k_2 at 165, 110, 96, 86 and 69 K, using the expression of Greenwald et al.[3] The open symbols are the data from Vakhtin et al.[43] at □(165 K), ○(110 K) and △(96 K). The filled symbols are the data for this study: ■(86 K) and ● (69 K).

Figure 9.
Second order plots of the decay rate k' versus [C_3H_4] for T = 86, 69 K (upper) and 298.8 K (lower). The individual error bars shown for each point incorporate the statistical error in the fitting of the exponential decay and the error in [C_3H_4] arising from density fluctuations in the supersonic gas flow, with the latter being the major contributor to the quoted uncertainty. The solid black lines are linear least-square fits of equation (E11) to the data, the gradients of which yield k_4, and the solid grey lines represent the 95% confidence limits of the fitted line.

References

1. I. W. M. Smith and B. R. Rowe, *Acc. Chem. Res.*, 2000, **33**, 261 - 268.

2. I. W. M. Smith, A. M. Sage, N. M. Donahue, E. Herbst and D. Quan, *Faraday Disc.*, 2006, **133**, 137-156.

3. E. E. Greenwald, S. W. North, Y. Georgievskii and S. J. Klippenstein, *J. Phys. Chem. A*, 2005, **109**, 6031 - 6044.

4. I. W. M. Smith, *Chem. Soc. Rev.*, 2002, **31**, 137 - 146.

5. Y. L. Yung, M. Allen and J. P. Pinto, *Astrophys. J. Supplement Series*, 1984, **55**, 465 - 506.

6. H. B. Niemann, S. K. Atreya, S. J. Bauer, G. R. Carignan, J. E. Demick, R. L. Frost, D. Gautier, J. A. Haberman, D. N. Harpold, D. M. Hunten, G. Israel, J. I. Lunine, W. T. Kasprzak, T. C. Owen, M. Paulkovich, F. Raulin, E. Raaen and S. H. Way, *Nature*, 2005, **438**, 779-784.

7. E. L. H. Feuchtgruber, T. de Graauw, B. Bezard, T. Encrenaz and M. Griffin, *Nature*, 1997, **389**, 159-162.

8. J. I. Moses, E. Lellouch, B. Bezard, R. G. Gladstone, H. Feuchtgruber and M. Allen, *Icarus*, 2000, **145**, 166 - 202.

9. D. O. Ham, D. W. Trainor and F. Kaufman, *J. Chem. Phys.*, 1970, **53**, 4395 - 4396.

10. I. R. Sims, in *Research in Chemical Kinetics*, ed. G. H. R. G. Compton, Blackwell Science Ltd., Editon edn., 1997, vol. 4, pp. 121 - 149.

11. I. W. M. Smith, *Angew. Chem. Int. Ed.*, 2006, **45**, 2842-2861.

12. M. A. Smith, *Int. Rev. Phys. Chem.*, 1998, **17**, 35 - 63.

13. B. R. Rowe, G. Dupeyrat, J. B. Marquette and P. Gaucherel, *J. Chem. Phys.*, 1984, **80**, 4915 - 4921.

14. B. R. Rowe and J. B. Marquette, *Int. J. Mass Spectrom. Ion Processes*, 1987, **80**, 239 - 254.

15. I. R. Sims, J. -L. Queffelec, A. Defrance, C. Rebrion-Rowe, D. Travers, P. Bocherel and I. W. M. Smith, *J. Chem. Phys.*, 1994, **100**, 4229 - 4241.

16. P. L. James, I. R. Sims, I. W. M. Smith, M. H. Alexander and M. Yang, *J. Chem. Phys.*, 1998, **109**, 3882 - 3897.

17. D. Chastaing, P. L. James, I. R. Sims and I. W. M. Smith, *Faraday Disc.*, 1998, **109**, 165 - 182.

18. H. Sabbah, L. Biennier, I. R. Sims, Y. Georgievskii, S. J. Klippenstein and I. W. M. Smith, *Science*, 2007, **317**, 102-105.

19. F. Goulay, C. Rebrion-Rowe, L. Biennier, S. D. Le Picard, A. Canosa and B. R. Rowe, *J. Phys. Chem. A*, 2006, **110**, 3132-3137.

20. F. Goulay, C. Rebrion-Rowe, J. L. Le Garrec, S. D. Le Picard, A. Canosa and B. R. Rowe, *J. Chem. Phys.*, 2005, **122**. Art. no. 104307.

21. P. C. N. Daugey, B. Retail, M. Costes, A. Bergeat, G. Dorthe, *Phys. Chem. Chem. Phys.*, 2005, **7**, 2921-2927.

22. S. Lee, R. J. Hoobler and S. R. Leone, *Rev. Sci. Instrum.*, 2000, **71**, 1816 - 1823.

23. A. B. Vakhtin, S. Lee, D. E. Heard, I. W. M. Smith and S. R. Leone, *J. Phys. Chem. A.*, 2001, **105**, 7889 - 7895.

24. D. B. Atkinson and M. A. Smith, *Rev. Sci. Instrum.*, 1995, **66**, 4434 - 4446.

25. T. Spangenberg, S. Köhler, B. Hansmann, U. Wachsmuth, B. Abel and M. A. Smith, *J. Phys. Chem. A*, 2004, **108**, 7527 - 7534.

26. E. Vohringer-Martinez, B. Hansmann, H. Hernandez, J.S. Francisco, J. Troe and B. Abel, *Science*, 2007, **315**, 497-501.

27. P. A. Cleary, M. T. Baeza Romero, M. A. Blitz, D. E. Heard, M. J. Pilling, P. W. Seakins and L. Wang, *Phys. Chem. Chem. Phys.*, 2006, **8**, 5633 - 5642.

28. D. B. Atkinson and M. A. Smith, *J. Phys. Chem.*, 1994, **98**, 5797 - 5800.

29. D. E. Heard, J.B. Jeffries, G. P. Smith and D. R. Crosley, *Combustion and Flame*, 1992, **88**, 137-148.

30. P. H. Paul, *J. Quant Spectrosc. Radiat. Transfer*, 1997, **57**, 581 - 589.

31. J. Luque and D. R. Crosley, *LIFBASE: Database and spectral simulation*, (1999) SRI International Report MP 99-009.

32. A. B. Vakhtin, D. E. Heard, I. W. M. Smith and S. R. Leone, *Chem. Phys. Lett.*, 2001, **348**, 21 - 26.

33. J. Brooke Koffend and N. Cohen, *Int. J. Chem. Kinetics*, 1996, **28**, 79 - 87.

34. D-C. Kim, K. W. Lee and K-H. Jung, *J. Chem. Phys.*, 1998, **109**, 1698 - 1703.

35. S. K. Shin, C. Rhee and H. L. Kim, *Bulletin of the Korean Chemical Society*, 1998, **19**, 319 - 323.

36. A. B. Vakhtin, D. C. McCabe, A. R. Ravishankara and S. R. Leone, *J. Phys. Chem. A.*, 2003, **107**, 10642 - 10647.

37. G. L. Vaghjiani and A. R. Ravishankara, *J. Phys. Chem.*, 1989, **93**, 1948-1959.

38. E. E. Nikitin and J. Troe, *Phys. Chem. Chem. Phys.*, 2005, **7**, 1540 - 1551.

39. M. A. Blitz, D. E. Heard and M. J. Pilling, *J. Photochem. Photobiol. A: Chemistry*, 2005, **176**, 107 - 113.

40. C. Anastasi, I. W. M. Smith and D. A. Parkes, *J. Chem. Soc., Faraday Trans.*, 1978, **1**, 1693 - 1701.

41. A. V. Ivanov, S. Trakhtenberg, A. K. Bertram, Y. M. Gershenzon and M. J. Molina, *J. Phys. Chem. A*, 2007, **111**, 1632-1637.

42. J. W. Davies, N. J. B. Green and M. J. Pilling, *Proc. Combust. Inst.*, 1986, **126**, 373-379.

43. A. B. Vakhtin, J. E. Murphy and S. R. Leone, *J. Phys. Chem. A*, 2003, **107**, 10055 - 10062.

44. J. Troe, *J. Chem. Phys.*, 1979, **83**, 114-126.

45. J. V. Michael, D. F. Nava, R.P.Borkowski, W. A. Payne and L. J. Stief, *J. Chem. Phys.*, 1980, **73**, 6108-6116.

46. K. W. McKee, M. A. Blitz, P. A. Cleary, D. Glowacki, M. J. Pilling, P. W. Seakins and L. Wang, *J. Phys. Chem. A*, 2007, **111**, 4043-4055.

47. J. P. Senosiain, S. J. Klipperstein and J. A. Miller, *J. Phys. Chem. A*, 2005, **109**, 6045 - 6055.

48. J. B. Davey, M. E. Greenslade, M. D. Marshall, M. I. Lester and M. D. Wheeler, *J. Chem. Phys.*, 2004, **121**, 3009 - 3018.

49. R. B. Boodahians, I. W. Hall, F. S. Toby and R. P. Wayne, *J. Chem. Soc. Faraday Trans. 2*, 1987, **83**, 2073 - 2080.

50. R. Atkinson and S. M. Aschmann, *Int. J. Chem. Kinetics*, 1984, **16**, 259 - 268.

51. S. Hatakeyama, N. Washida and H. Akimoto, *J. Phys. Chem.*, 1986, **90**, 173 - 178.

52. J. N. Bradley, W. Hack, K. Hoyermann and H. Gg. Wagner, *J. Chem. Soc. Faraday Trans. 1*, 1973, **69**, 1889 - 1898.

53. L. Y. Yeung, M. J. Pennino, A. M. Miller and M. J. Elrod, *J. Phys. Chem. A*, 2005, **109**, 1879 - 1889.

54. B. Bohn and C. Zetzsch, *Phys. Chem. Chem. Phys.*, 1999, **1**, 5097 - 5107.

55. A. Morikawa and R. J. Cvetanovic, *J. Chem. Phys.* 1969, **52**, 3237-3239.

Table 1.

Details of Laval nozzles used in this work. The carrier gas is N_2.

Design expansion temperature / K	Design gas density /10^{16} molecule cm^{-3}	Flow rate / sccm [d]	Measured Mach number [a]	Measured expansion temperature / K [b]	Measured gas density / 10^{16} molecule cm^{-3} [c]	Gas velocity in flow / ms^{-1}
106	5.0	1688 ± 17	3.5 ± 0.1	86 ± 4	3.85 ± 0.41	663 ± 30
71	5.0	1557 ± 15	4.05 ± 0.11	69 ± 3	3.67 ± 0.43	689 ± 70

[a] Calculated from impact pressure measurement and iterative solution to equation (E2)
[b] Calculated from measured Mach number and equation (E3). Uncertainty is 1σ from the mean of all values obtained along the supersonic flow.
[c] Calculated from measured Mach number and equation (E5). Uncertainty as for temperature.
[d] Uncertainty obtained by calibration (~ 1%)

Table 2.

Summary of rate coefficient measurements for the OH + ethene reaction. The carrier gas is N_2.

Temperature / K	Gas density / 10^{16} molecule cm^{-3}	Range of [C_2H_4] / 10^{14} molecule cm^{-3}	k_2 / cm^3 molecule^{-1} s^{-1} [a]
86 ± 4	3.84 ± 0.41	0.62 – 4.09	(2.12 ± 0.12) × 10^{-11}
69 ± 3	3.67 ± 0.43	0.37 – 2.93	(3.22 ± 0.46) × 10^{-11}

[a] Quoted uncertainties are at the 95% confidence limit taking into systematic errors (for example, pressure and mass flow controller readings).

Table 3.

Summary of rate coefficient measurements for the OH + propyne reaction. The carrier gas is N_2.

Temperature / K	Gas density / 10^{16} molecule cm^{-3}	Range of [C_2H_6] / 10^{14} molecule cm^{-3}	k_4 / cm^3 molecule^{-1} s^{-1} [a]
298.8 ± 0.1	3.26 ± 0.07	3.3 – 65.6	(3.11 ± 0.09) × 10^{-12}
86 ± 4	3.64 ± 0.39	0.37 – 3.54	(5.02 ± 1.11) × 10^{-12}
69 ± 3	3.66 ± 0.48	0.73 – 3.70	(5.08 ± 0.65) × 10^{-12}

[a] Quoted uncertainties are at the 95% confidence limit taking into systematic errors (for example, pressure and mass flow controller readings).

Figure 1(a).

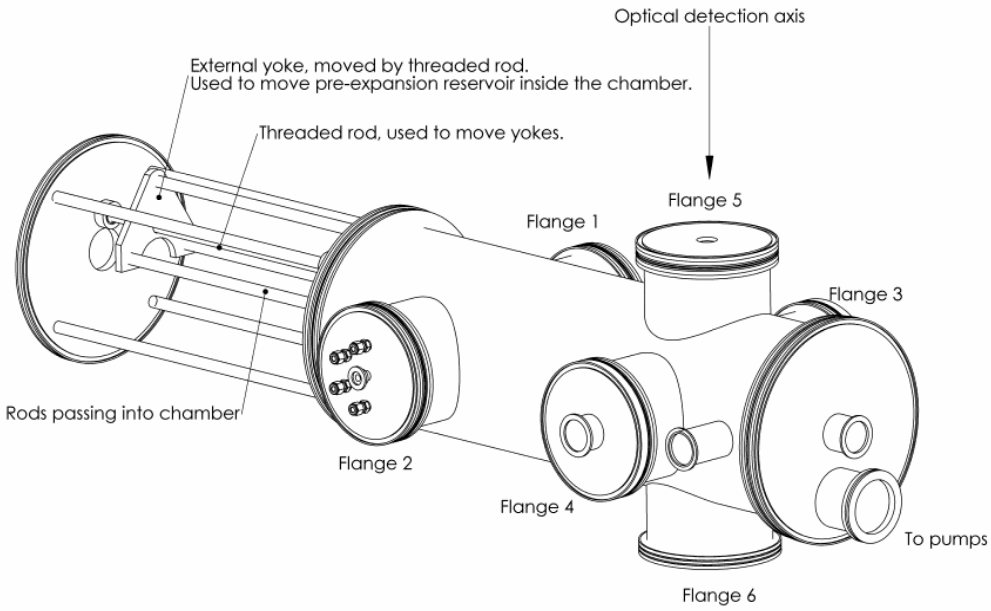

Figure 1(b).

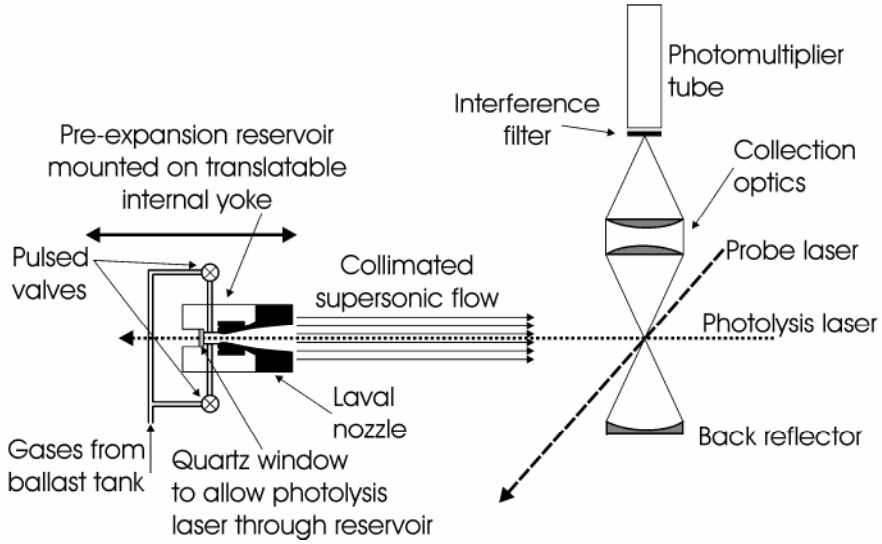

Figure 2.

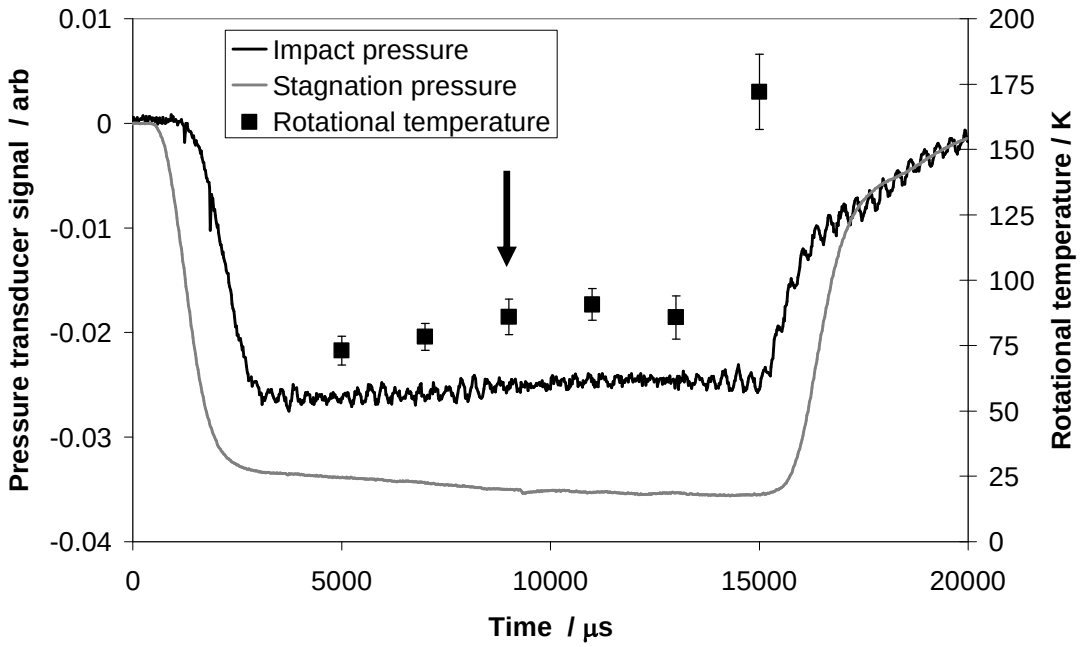

Figure 3.

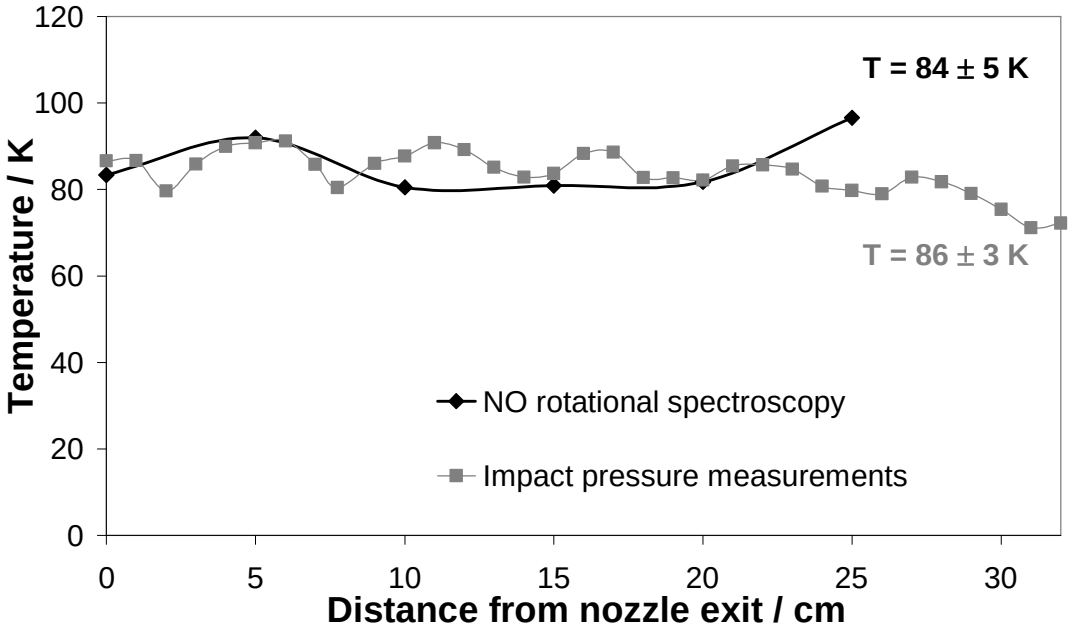
120
100
80
60
40
20
0
Temperature / K
0
5
10
15
20
25
30
Distance from nozzle exit / cm
T = 84 ± 5 K
T = 86 ± 3 K
NO rotational spectroscopy
Impact pressure measurements

Figure 4.

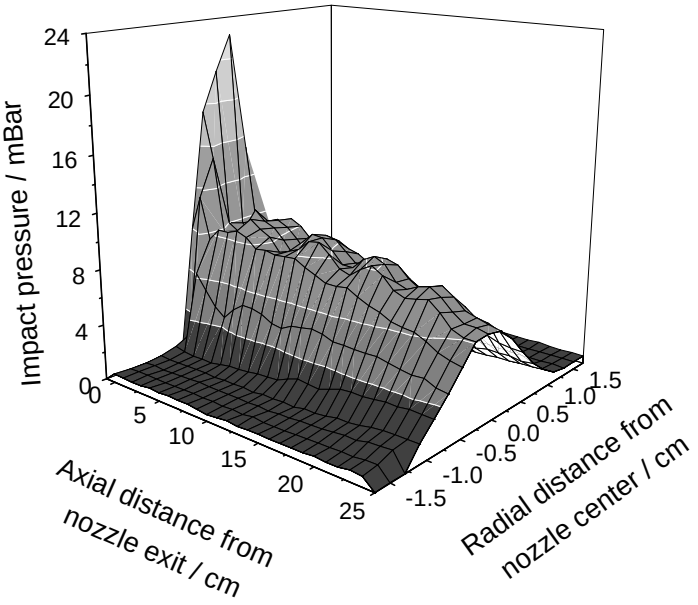

Figure 5(a).

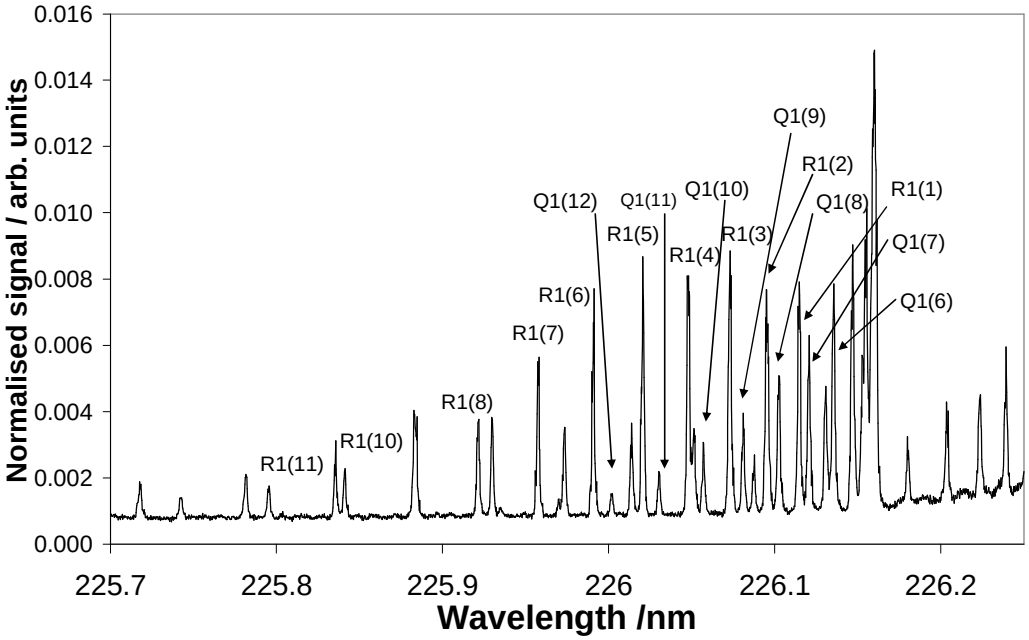

Figure 5(b).

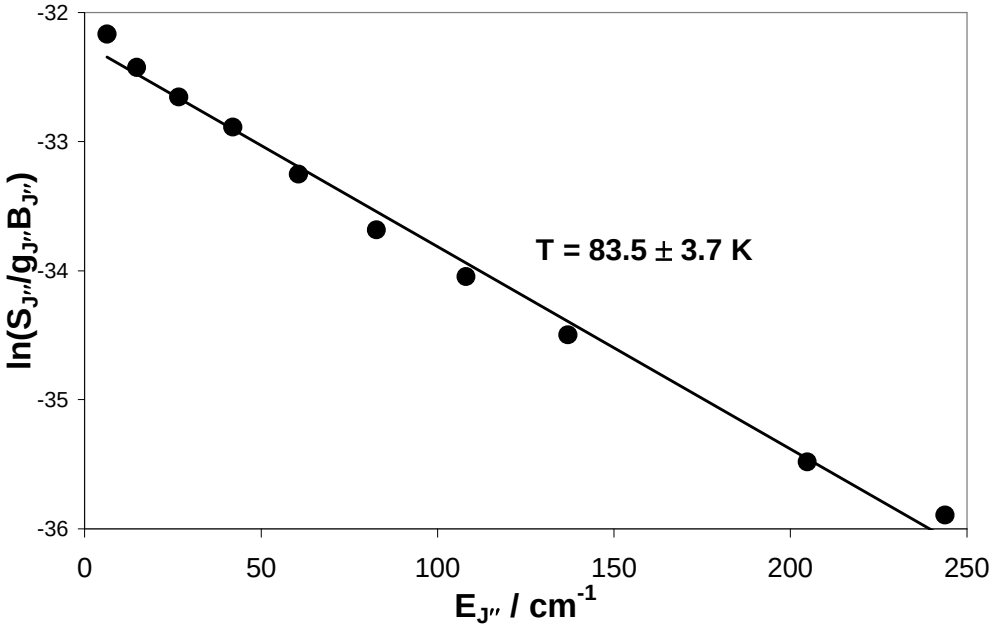

Figure 6.

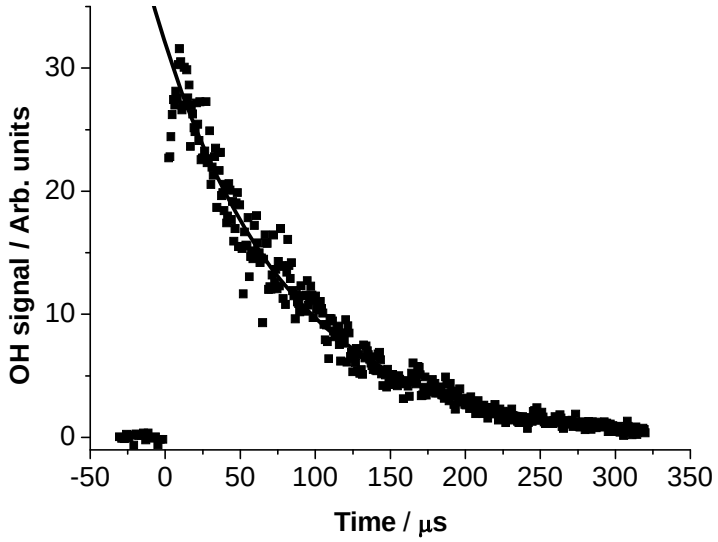

Figure 7.

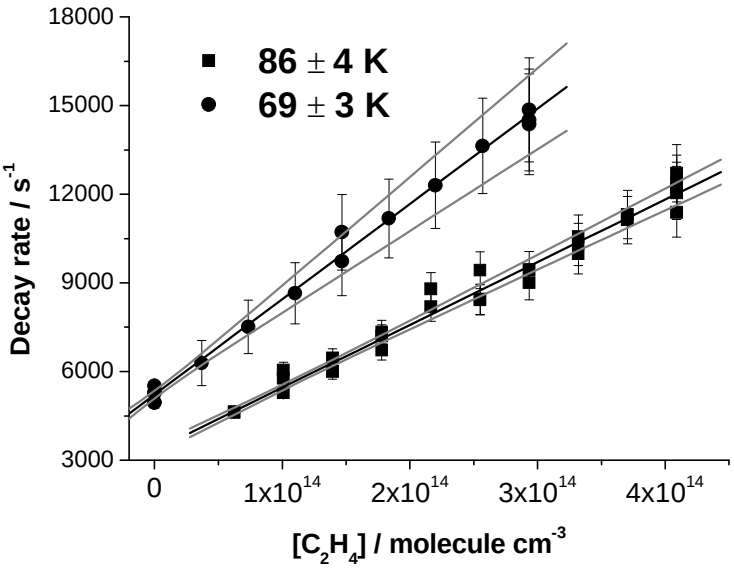
86 ± 4 K
69 ± 3 K
Decay rate / s-1
18000
15000
12000
9000
6000
3000
0
1x10^14
2x10^14
3x10^14
4x10^14
[C2H4] / molecule cm-3

Figure 8 (a).

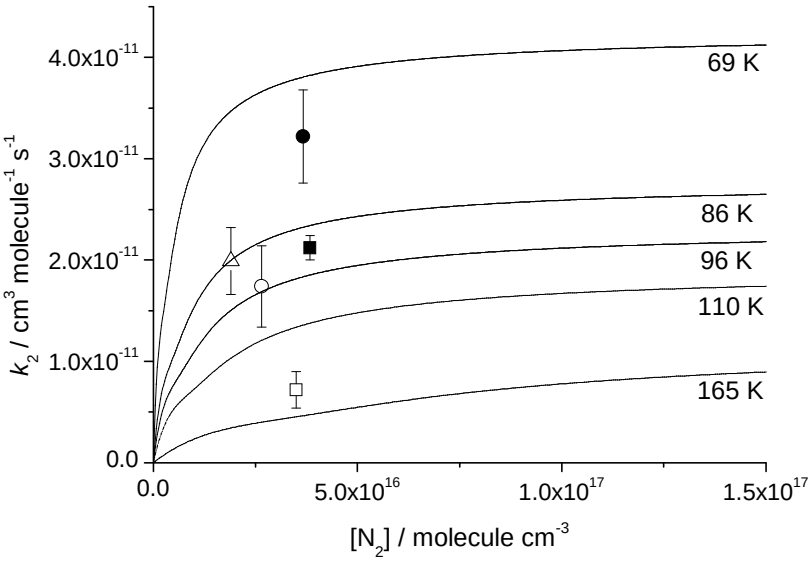

Figure 8(b).

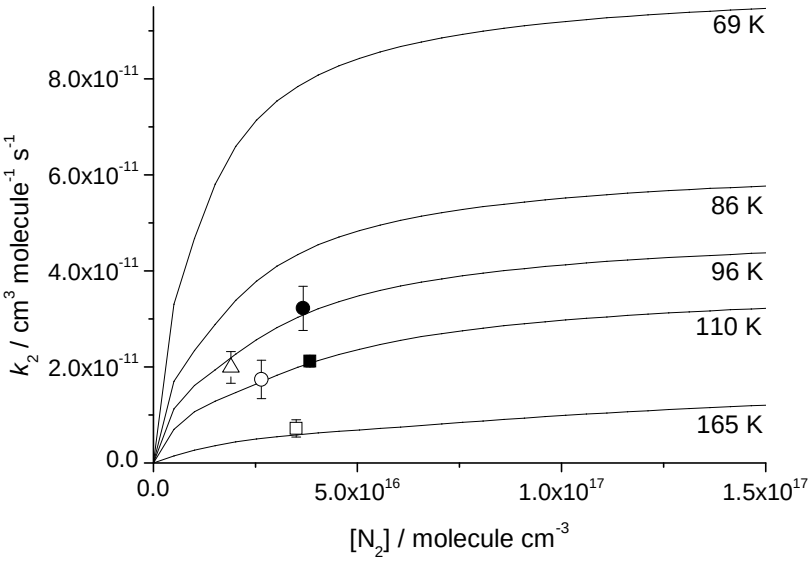

Figure 9.

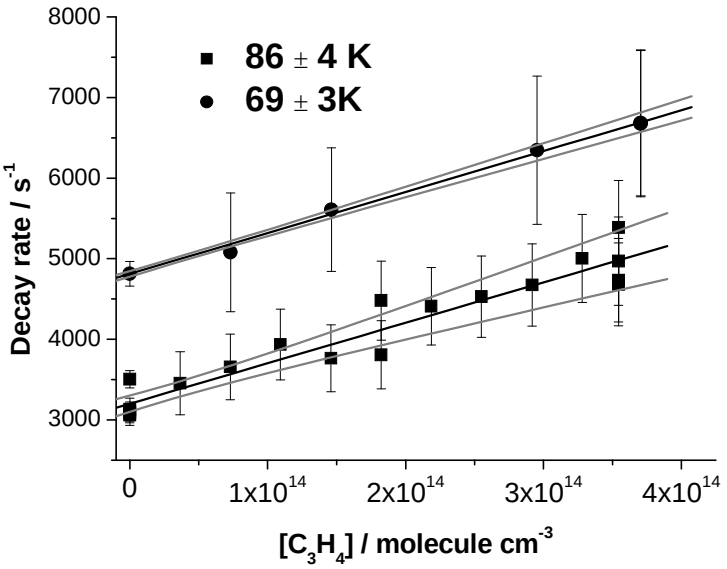
86 ± 4 K
69 ± 3K
Decay rate / s-1
8000
7000
6000
5000
4000
3000
0
1x10^14
2x10^14
3x10^14
4x10^14
[C3H4] / molecule cm-3

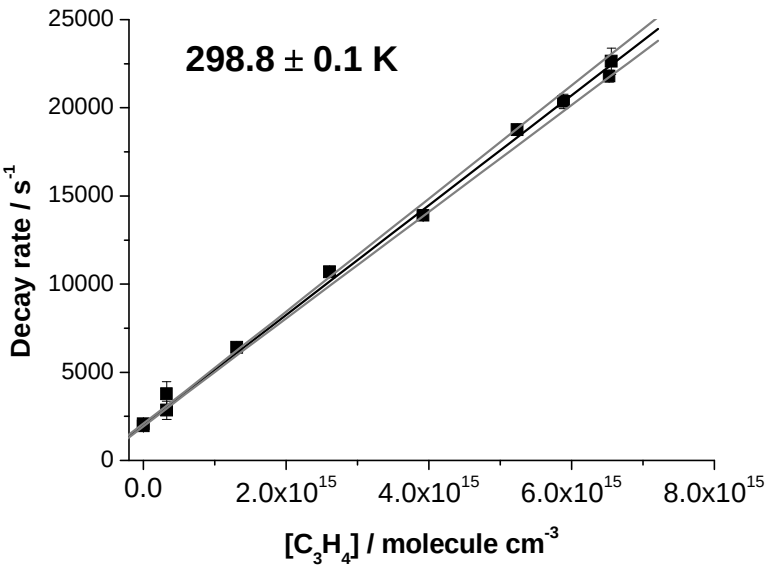
298.8 ± 0.1 K
Decay rate / s-1
25000
20000
15000
10000
5000
0
0.0
2.0x10^15
4.0x10^15
6.0x10^15
8.0x10^15
[C3H4] / molecule cm-3